

Centrifugal force driven low frequency modes in spherical tokamak

G.Z. Hao,^{1*} W.W. Heidbrink,¹ Y.Q. Liu,² S.X. Yang,³ D. Liu,¹ E.D. Fredrickson,⁴ Y. Ren,⁴
R. Bell,⁴ N.A. Crocker,⁵ M. Podestà,⁴ F. Wang,³ K. Tritz,⁶ A.K. Wang,⁷ and M. Xu⁷

¹*University of California, Irvine, California 92697, USA*

²*General Atomics, San Diego, California 92186-5608, USA*

³*Dalian University of Technology, Dalian 116024, China*

⁴*Princeton Plasma Physics Laboratory,
Princeton, New Jersey 08540, USA*

⁵*University of California, Los Angeles, California 90095, USA*

⁶*Johns Hopkins University, Baltimore, Maryland 21218, USA*

⁷*Southwestern Institute of Physics, Chengdu 610041, China*

Abstract

There is a longstanding issue on the physical nature of a low frequency (<50 kHz) MHD instability observed at the early phase of the discharges of a spherical tokamak (ST) - the National Spherical Torus Experiment (NSTX) (Ono *et al* 2000 *Nucl. Fusion* **40** 557). This letter provides evidence that low frequency modes in spherical tokamaks are often driven by the rapid plasma flow. The centrifugal force associated with toroidal plasma flow is identified as the key physics mechanism for generating this instability located in the plasma core region. Positive mode identification between toroidal modeling and experiments is achieved for the mode frequency, the mode internal structure, as well as the threshold flow value for the mode onset. The threshold flow value weakly depends on the precise value of safety factor and the mode is located around the location of sharp density gradient. More importantly, since the achievable rotation value on NSTX is comparable with that for future Component Test Facilities (CTF) based on ST (Peng *et al Plasma Phys. Control. Fusion*,**47**,B263), the presented results in this work are helpful for the conceptual design of ST-CTF to avoid the instability driven by fast plasma flow.

Introduction.— It is well known that toroidal rotation can ameliorate or suppress many performance-limiting magneto-hydrodynamic (MHD) instabilities, such as resistive wall modes [1] and tearing modes [2], in magnetically confinement fusion devices. However, when the plasma flow is too fast, MHD instability, such as Kelvin-Helmholtz (KH) instability, can be driven [3] and, it will reduce the plasma performance. Furthermore, centrifugal forces associated with fast toroidal flow of the plasma can drive a kind of interchange-like instability [4, 5]. Owing to the small plasma volume per unit of Neutral Beam Injection (NBI) power, spherical tokamak (ST) plasmas can rotate toroidally at a significant fraction of the Alfvén speed [6]. This letter reports conclusive identification of the role of centrifugal force in driving a class of low frequency internal instabilities in an ST - the National Spherical Torus Experiment (NSTX) [7, 8]. This type of instability is likely to occur in future STs, such as the Component Test Facility (ST-CTF) [9], in which the plasma Alfvén Mach number is ~ 0.4 , which is comparable with the value on NSTX. The results presented in this work will help ST-CTF avoid instabilities driven by fast plasma flow, such as through controlling the density profile to mitigate the centrifugal force in the core plasma region. In addition to its importance for STs, MHD instabilities driven by fast flow or flow shear are common and play important roles in naturally occurring plasmas. For instance, KH instability driven by sheared flows [10] was utilized to explain the anomalous transport in the solar-wind magnetosphere [11], as well as to account for the source of inhomogeneous mixing elements in nova explosions [12]. The electrostatic interchange instability driven by fast flow was observed in a magnetic dipole device [13].

During NSTX discharges, low frequency (< 50 kHz) instabilities are often observed. The occurrence of these modes often significantly reduces the plasma performance, leading to β_N saturation, fast-ion redistribution/loss and the plasma current redistribution [8, 14–16]. Here, $\beta_N \equiv \beta_T a B_T / I_p [\% \text{mT/MA}]$ is the normalized beta, with $\beta_T \equiv 2\mu_0 \langle p \rangle / B_T^2$ being the volume averaged dimensionless plasma pressure. One class of low frequency modes have previously been successfully identified as an ideal external kink instability [17], which is unstable due to reduced ideal-wall β_N limits by the combined influence from both toroidal plasma rotation and fast ion kinetic contribution. During the late phase of certain NSTX discharges, an internal mode structure was empirically established, based on the best fitting between the simulated and measured Ultra soft-x ray (USXR) fluctuations [15]. Yet another class of low frequency modes were identified as energetic particle modes [18], with the mode

onset frequency being larger than the plasma rotation frequency.

On the other hand, many NSTX plasmas suffer a low frequency instability during the early phase of discharge. The frequency of the instability typically matches well the plasma toroidal rotation frequency at the radial location of the mode, which is usually within the major radius of $R < 120$ cm. At the saturated state, this kind of mode induces the drop of neutron rate by $\sim 20\%$ [19], the drop of beam-driven current by $\sim 40\%$ [19] and the toroidal beta (β_T) drop by $\sim 7\%$ [14, 19]. In NSTX, the neutron rate drop corresponds to a similar drop of the population of the most energetic ions [20]. In addition, the fast-ion redistribution and the accompanied beam-driven current are sensitive to the mode structure of the instability [19]. Therefore, in order to precisely simulate the plasma performance affected by this kind of internal instability, it is important to identify the onset conditions.

There has been a longstanding debate of what causes the onset of this instability, which clearly has no external kink structure. Various hypotheses (e.g. peeling, tearing, infernal modes) have been put forward but rejected due to lack of matching all signatures observable in experiments, as will be discussed later in the paper. Here, we identify the fast plasma flow induced centrifugal force as the key driving mechanism for this class of instability.

Experimental observation.— A typical discharge of NSTX, with the machine major radius of $R_0 = 0.85$ m and the plasma minor radius of $a = 0.65$ m, operates at the toroidal magnetic field of $B_T \leq 0.55$ T and the plasma current I_p up to 1.5 MA. The plasma cross section has elongation $\kappa = 1.8 - 2.4$ and triangularity $\sigma = 0.3 - 0.8$. The beam heating power P_{NBI} is up to 6 MW.

Figure 1 shows an example of an NSTX discharge at plasma current of $I_p = 0.9$ MA and with the input neutral beam power of $P_{NBI} = 2$ MW [Fig. 1 (a)]. An $n = 1$ low frequency (low-f) mode occurs at 331 ms [Fig. 1 (c) and (d)]. Here, n is the toroidal mode number of the instability. The onset mode frequency matches the plasma toroidal rotation frequency measured at the major radius of $R = 116$ cm (the magnetic axis position is $R_{axis} = 101$ cm). During the frequency decay phase of the $n = 1$ mode, an $n = 2$ perturbation also develops. In the saturation phase, the neutron rate is significantly reduced compared to that predicted by the TRANSP simulation [Fig. 1 (b)], without any anomalous diffusion for fast ions [21]. Meanwhile, the $n = 1$ toroidal Alfvén eigenmode (TAE) bursts appear. Both the neutron rate change and the TAE excitation suggest that the saturated (both $n=1$ and 2) low-f modes substantially redistribute fast ions. Furthermore, Refs. [19, 22], where

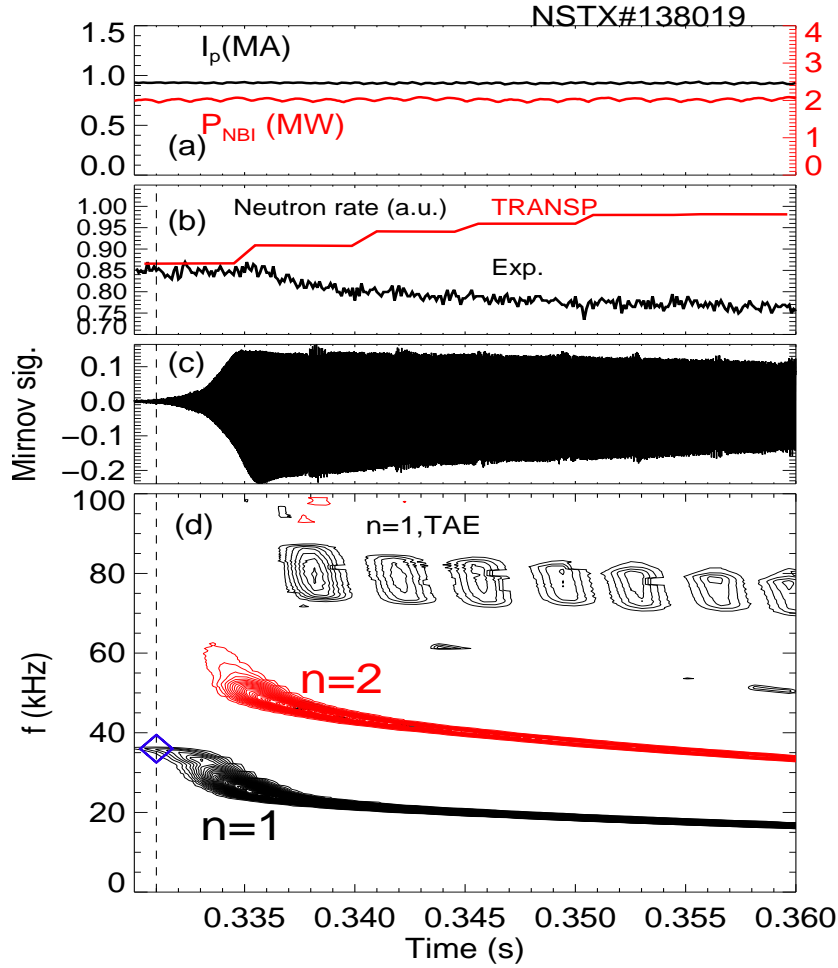


FIG. 1. Time traces of the NSTX discharge 138019 with (a) the plasma current and NBI heating power, (b) the measured (black) and predicted (red) neutron rate, (c) the raw data and (d) spectrum of the Mirnov signal. Dashed line denotes the onset time of the $n=1$ low- f mode, with symbol \diamond indicating the plasma rotation frequency at $R=116$ cm before the mode onset.

the mode structure was approximated by a simple analytical model, also reported that this class of low- f mode enhances the fast ion loss.

Based on the selection criteria that the onset mode frequency matches the plasma rotation frequency at a certain radial location and the identified mode position is located in the core region, a database is established, where $\beta_N = 2 - 5$, $P_{NBI} = 1.8 - 6$ MW and the toroidal rotation at R_{axis} varies between 25-45 kHz. The low- f mode significantly damps the plasma core rotation, with one example shown in Fig. 2 (a). The process occurs within ~ 10 ms time interval. Outside the core, the plasma rotation slightly increases. Analysis of the

database shows that the damping of the core rotation is a generic feature [Fig. 2 (c)]. The database also indicates that the radial location of the mode, identified by matching the mode frequency to the plasma rotation frequency, is localized in the core region, near $R = 115$ cm [Fig. 2 (b)]. At the mode's radial location, the centrifugal force ($\propto \partial(\rho\Omega^2)/\partial R$), estimated at a time slice just before the observed mode onset, is also relatively large [Fig. 2 (d)]. This provides the first indication of the role of the centrifugal force on the mode onset. Here, the plasma rotation profile is measured by charge exchange recombination spectroscopy with 10 ms temporal resolution [23]. The plasma density ρ is measured by a multi-point Thompson scattering system with about 16 ms resolution. The present temporal resolution of these diagnostics is not sufficient to determine the plasma rotation and density profiles at the exact onset time of the low-f mode, nor sufficient to determine the rotation profile evolution during the mode decay. Nevertheless, the database shows that the low-f mode is generally localized in the core region of the plasma, where the centrifugal force is relatively large.

Modeling framework.—In order to gain a better physics understanding of the role of the centrifugal force on the $n = 1$ low-f mode, we employ the full toroidal MHD eigenvalue code MARS-F [24, 25]. The code includes, among other physics, toroidal flow of the plasma as well as a resistive plasma model. MARS-F interfaces with a static toroidal equilibrium solver CHEASE [26], which in turn utilizes results from the equilibrium fitting code LRDFIT [27]. LRDFIT assumes an inductance-resistance 2D axisymmetric circuit model for the tokamak equilibrium reconstruction, where the Grad-Shafranov equilibrium is enforced and is constrained to fit to various diagnostic data. In this work, the experimental constraints include the magnetics data, the plasma toroidal rotation, the motional stark effect (MSE) including electric potential correction, and the assumption of electron temperature being a flux function.

MARS-F solves, among other MHD equations, the following perturbed momentum equation

$$\begin{aligned} \rho(\gamma - i\omega_r + in\Omega)^2 \boldsymbol{\xi} = & -\nabla p + \mathbf{j} \times \mathbf{B} + \mathbf{J} \times \mathbf{Q} \\ & + 2\rho(\gamma - i\omega_r + in\Omega)\Omega \hat{\mathbf{Z}} \times \boldsymbol{\xi} - R\hat{\mathbf{R}}\nabla \cdot (\rho\Omega^2 \boldsymbol{\xi}) \end{aligned} \quad (1)$$

where γ and ω_r are the mode growth rate and real frequency, respectively. ρ , \mathbf{B} and \mathbf{J} are the equilibrium density, magnetic field and plasma current, respectively. Ω is the plasma toroidal rotation frequency. $\boldsymbol{\xi}$, p , \mathbf{j} and \mathbf{Q} are the plasma displacement, perturbed pressure, current and magnetic field, respectively. The unit vectors along the major radius and the

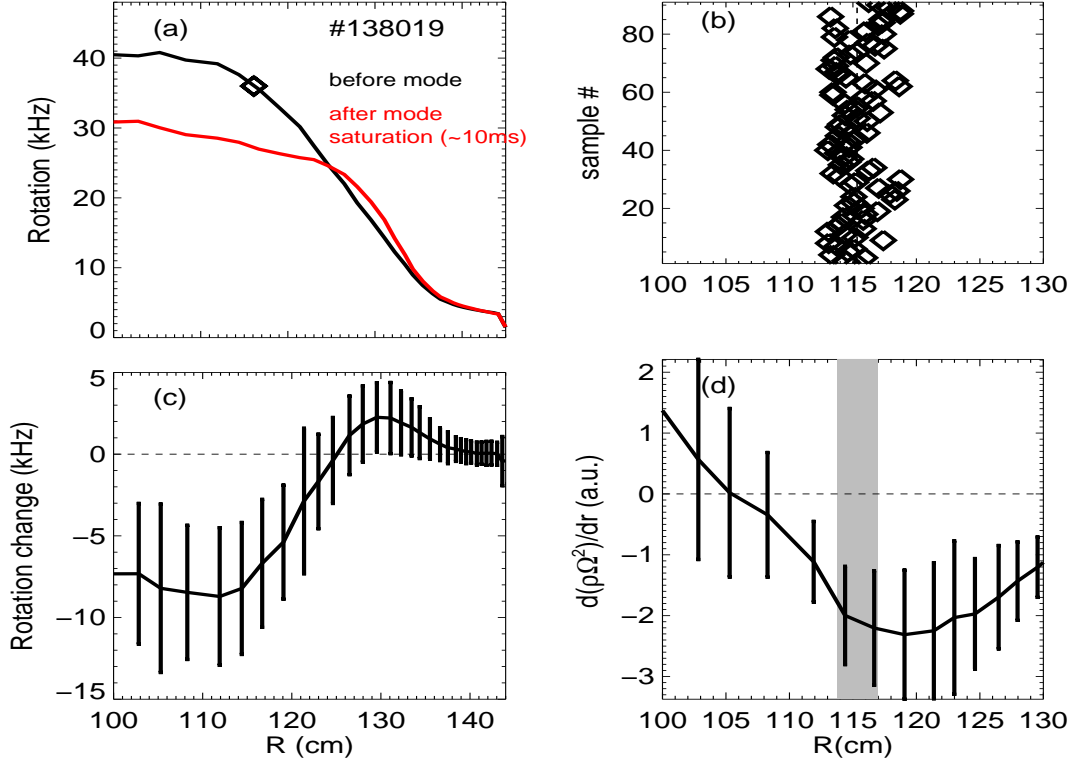


FIG. 2. (a) Plasma toroidal rotation frequency before (black) and after (red) the low-f mode onset in discharge 138019, with symbol ' \diamond ' labeling the measured mode frequency at onset in laboratory frame. (b) Symbols denote the radial position where the mode frequency matches the plasma rotation frequency, for conditionally chosen 92 NSTX discharges. The vertical dashed line indicates the mean value of the matching radius. (c) The low-f mode induced change of rotation, averaged over shots in the database. (d) An indicator of the centrifugal force averaged over shots in the database, with the shaded region denoting the mode location. Error bars in (c) and (d) denote the standard derivation.

vertical direction are $\hat{\mathbf{R}}$ and $\hat{\mathbf{Z}}$, respectively. The mode toroidal number $n = 1$ is considered in MARS-F computations. The two inertial terms from the right hand side of the equation, $\mathbf{F}_{cl} \equiv 2\rho(\gamma - i\omega_r + in\Omega)\Omega\hat{\mathbf{Z}} \times \boldsymbol{\xi}$ and $\mathbf{F}_{cf} \equiv -R\hat{\mathbf{R}}\nabla \cdot (\rho\Omega^2\boldsymbol{\xi})$, represent the coriolis and centrifugal forces, respectively. In the simulation results reported below, all the frequencies are normalized by the Alfvén frequency $\omega_A \equiv 1/\tau_A$, with τ_A being the toroidal Alfvén time at the magnetic axis.

Key results.— In the following, we report key results of comparing the MARS-F modeling with experiments for (i) the rotation threshold $\Omega_c\tau_A$ for driving the low-f mode, (ii) the onset mode frequency, and (iii) the internal structure of the mode.

We pay special attention to various uncertainty and sensitivity issues in the mode identification. An important uncertainty in the equilibrium reconstruction is the lack of constraint on the pressure profile in LRDFIT, resulting in uncertainty in the reconstructed safety factor profile and uncertainty of the predicted β_N . Furthermore, we also study the dependence of the results on an uncertainty in the measured plasma core density profile. Finally, other physics effects in addition to the centrifugal force in the stability model, such as the plasma resistivity and the drift kinetic effect of fast ions, may also change the numerical results and will thus also be examined.

Figure 3 reports several examples of the MARS-F computations for an NSTX discharge, and compares with the experimental results. By specifying different basis functions for the pressure gradient [27] in LRDFIT (while still applying the MSE and other data constraints), slightly different q -profiles are obtained in the plasma core, as shown by the solid curves in Fig. 3(a). The sensitivity study is expanded by including one more case (dash-dotted curve in Fig. 3(a)) with rescaled q_{\min} , based on the case labeled 'QP1' with $q_{\min} = 2.1$. The measured density and rotation profiles as shown in Fig.3 (b) are utilized in MARS-F computation. The uncertainty of measured density is of the order of 4%, which significantly affects the computed instability growth rate, as will be shown. The uncertainty of the measured rotation is typically smaller than 1%, which is ignored in this study.

Figure 3(c) shows that, with various choices of the core safety factor profiles, an $n = 1$ instability always occurs when the plasma rotation frequency exceeds a critical value $\Omega_c\tau_A$. Here, the measured rotation profile is used, with the amplitude scanned. This shows a robust drive of the instability against uncertainties in determining the core q -profile. On the other hand, the threshold rotation frequency, $\Omega_c\tau_A$, depends on the q -profile. However, $\Omega_c\tau_A$ almost does not depend on q_{\min} when the q -profile is fixed. For the case of QP1-model, the corresponding $\Omega_c\tau_A$ value is 0.262, which is close to the measured plasma rotation frequency (0.236) just before the $n = 1$ mode onset. The computed mode frequency (0.24) is also consistent with the experimental value (0.22). Overall, taking into account the variations in the q -profile, the computed linear stability threshold exceeds the observed value by $\leq 25\%$. In addition, it is found that the Coriolis force has a stabilization effect on the mode driven

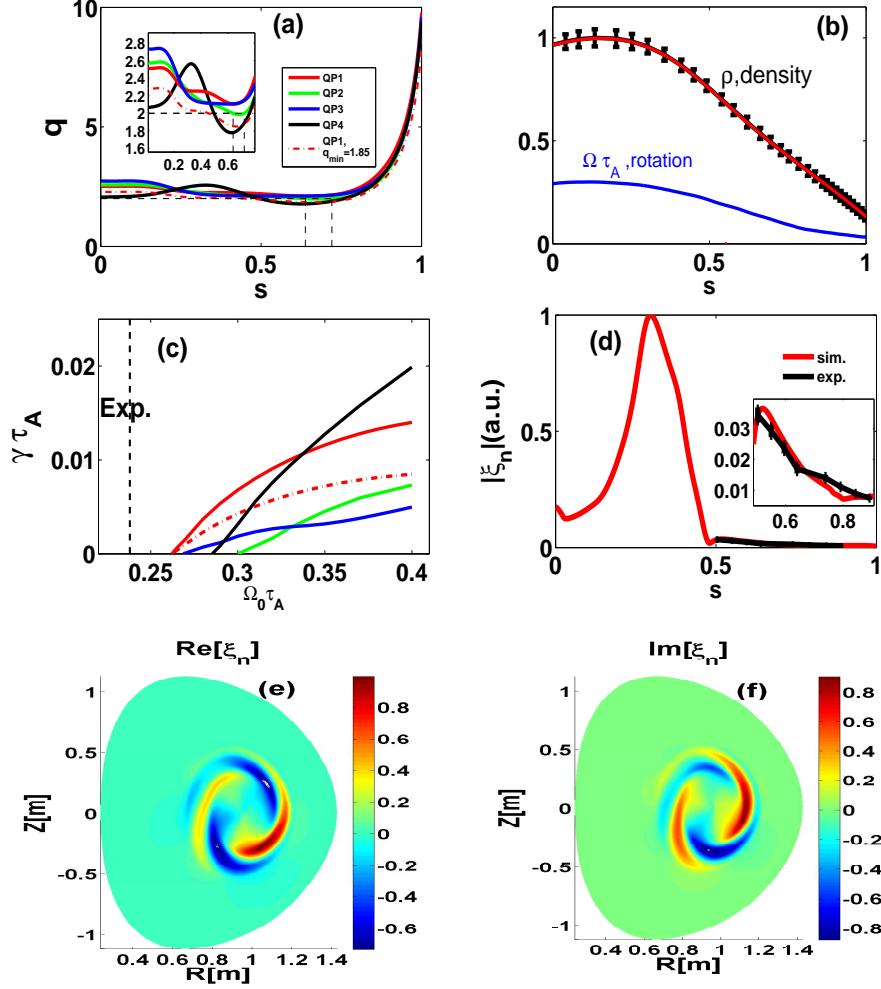


FIG. 3. MARS-F modeling input and results for NSTX discharge 137617, with (a) the reconstructed (solid curves) and rescaled (dash-dotted curves) safety factor profiles, (b) the measured ion density profile normalized to its maximum (black curve with error bars) and the fitted one used in computation (red). Blue curve is the fitted experimental rotation profile. (c) The mode growth rate with varying amplitude of toroidal rotation frequency $\Omega_0\tau_A$ and with different q -profiles as shown in (a). The vertical dashed line denotes the measured plasma rotation frequency for the mode onset in experiment. Shown in (d) is the computed normal displacement (red) plotted together with that reconstructed from the reflectometer data (black). The horizontal axis in (a,b,d) is the plasma minor radius labeled by the square root of the normalized equilibrium poloidal flux, $s \equiv \sqrt{\psi_p}$. (e) and (f) show the real and imaginary parts of computed plasma normal displacement in the (R,Z) -domain, for the case of "QP1" and $\Omega_0\tau_A = 0.30$.

by the centrifugal force.

In fact the mode peaks at $s = 0.3$ [Fig.3(d)], being far away from the $q_{min}(= 2.1)$ position of $s=0.66$. This shows that the mode here is different from the infernal mode, which is often localized at local minimum of q and when q_{min} is sufficiently close to an integer. The infernal mode instability is thought to be responsible for the long-lived mode (LLM) observed on MAST [28], NSTX [29, 30] and recently on HL-2A [31].

The shape of the modeled plasma displacement along the mid-plane is consistent with the reflectometer data [Fig.3(d)], which are available only in the outboard side of the plasma column in the studied discharge. It is experimentally confirmed that the perturbation near the plasma edge is very weak, and becomes stronger towards the inside of the plasma. We also mention that the mode peaks at $s \approx 0.3$ for all cases shown in Fig.3(a). Fig.3(e) and (f) indicate that the dominant harmonic for this instability is $m/n = 2/1$ (m is the poloidal mode number) and the perturbation is localized in the plasma core region.

In order to validate the mode structure in the plasma core region, we utilize the USXR data. The MARS-F computed plasma displacement is used to synthesize the numerical USXR signal, to be compared with the direct measurements. Since there are no USXR data available for discharge 137617, we choose a similar discharge 138019. The USXR emission mainly depends on the electron density n_e , temperature T_e and the impurity density n_c . The USXR signal, produced from equilibrium emission, is line-integrated along each chord, or the line of sight l , as $S_0 = \int \epsilon_0(\psi_p) dl$ with $\epsilon_0 = n_e n_c f(T_e)$. Here, $f(T_e)$ is a weighting function, which is tuned to best match the simulated S_0 profile with the measurements [Fig.4(a)]. The USXR fluctuation, associated with the mode perturbation, is then represented as $S_1(t) = \int \delta\epsilon_0(\psi_p, \theta, t) dl = \int \text{Re}(e^{i\omega_r t} \xi \cdot \nabla s) \partial\epsilon_0(\psi_p) / \partial s dl$. The perturbation $\delta\epsilon_0(\psi_p, \theta, t = 0)$ is plotted in Fig. 4(b), together with the geometry of the USXR chords in NSTX.

To simulate the USXR fluctuation, we use the computed mode structure with growth rate $\gamma\tau_A = 4.2 \times 10^{-3}$, which is comparable to the experimental value of $\gamma\tau_A = 6.2 \times 10^{-3}$ at 332 ms. This is the time slice when the USXR fluctuation is extracted from measurements. A key observation is that the simulated integrated USXR fluctuation S_1 exhibits an inversion near chord #5 [Fig.4(d)], again being consistent with the measurements [Fig.4(c)]. Moreover, the simulated spectrum between chords 1-4 and chords 7-9 also agrees well with the measurements. Along the outer chords #10-15, both the simulated and measured USXR fluctuations are very weak (hence not plotted here). We also point out that the simulated USXR fluctuation using mode structures with much lower or much larger growth rates poor-

ly agrees with measurements. This is largely due to the fact that mode structure becomes narrower/broader as the growth rate decreases/increases. Another interesting finding is that the simulated inversion radius is fully determined by the radial location of the mode. Figure 4 thus shows convincing evidence for positive identification of the core structure of the mode.

We should also point out that the simulated USXR signal at chord #5 (#6) is relatively stronger (weaker) as compared to the measurements. This is possibly due to the uncertainty associated with the weighting function $f(T_e)$.

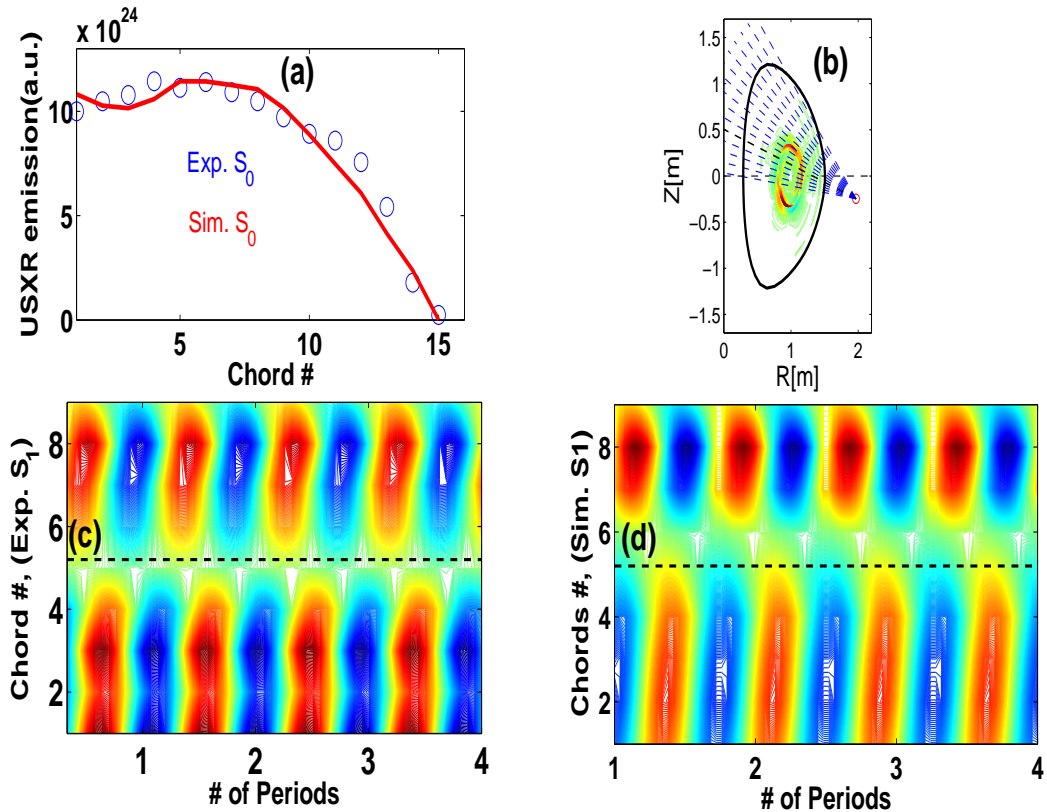


FIG. 4. Comparison of (a) the experimental (blue open circles) and simulated (red) USXR signal from the equilibrium emission ϵ_0 . (b) The simulated USXR fluctuation $\delta\epsilon_0$ plotted together with the USXR geometry (15 chords denoted by dashed lines). (c) The measured and (d) simulated line-integrated USXR fluctuation, in which 'Period' means a period of the oscillation of USXR fluctuation as a function of time.

The radial location of the computed internal mode depends sensitively on the density profile [Fig. 5 (a)]. Here, we fix the plasma rotation profile as well as the amplitude

($\Omega_0\tau_A = 0.3$), while the density profile is varied. It is evident that the mode tends to locate in the region where the density gradient is relatively large. The mode frequency, not shown here, follows the local plasma rotation at the mode location. It should be noted that the q -profile is kept the same for different cases shown in Fig. 5 (a). The results thus show that the density profile plays the dominant role on the mode location. Furthermore, the more computations suggest that the other inertial effects (such as the Coriolis force) in addition to the centrifugal force also have the contribution to determine the exact mode position. In addition, the critical rotation frequency, $\Omega_c\tau_A$, decreases as the density gradient increases (roughly equivalent to the increase of the centrifugal force) near the mode location [Fig. 5 (b)].

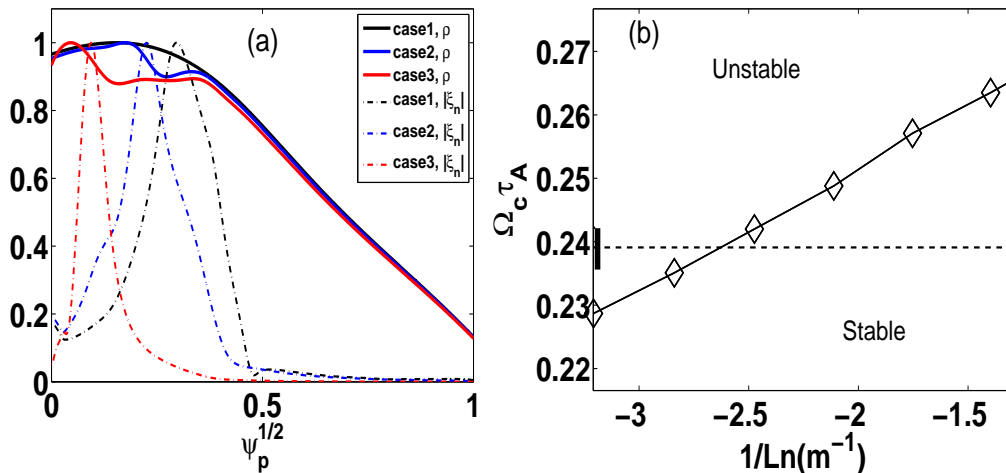


FIG. 5. Plot (a) shows the computed normal displacement (dash-dotted curves) for three choices of the normalized plasma core density profile. The displacement amplitude is arbitrarily rescaled. Plot (b) shows the computed critical rotation $\Omega_c\tau_A$ (solid curve) with varying equilibrium density gradient at $s = \sqrt{\psi_p} = 0.3$, denoted here by $1/L_n \equiv (d\rho/dR)/\rho$. The experimental $1/L_n$ value is in the region of $[-3.5, 1.4]$. The horizontal dashed line and the black bar denote the experimentally observed critical rotation frequency and its uncertainty. Considered here is the NSTX discharge 137617.

Discussion.— The ideal MHD modeling results presented so far provide quantitative identification of the $n = 1$ low- f internal instability in the NSTX experiments. We also

examined effects of additional physics on the mode onset, in particular that of the plasma resistivity and the drift kinetic effects from energetic ions due to NBI. The plasma resistivity has almost no effect on the mode growth rate and the mode structure for the studied cases here. In addition, since the pressure constraint is not included in LRDFIT equilibrium fitting, it is worth to estimate the influence of the plasma pressure on the mode. The computed results show that the pressure destabilizes the mode and the increase of β_N by 10% induces the decrease of threshold value $\Omega_c \tau_A$ by 4%. for driving the mode.

Kinetic effects from fast ions are also found to be not important for the occurrence of the low-f instability. Non-perturbative, MHD-kinetic hybrid computations using the MARS-K code [32] show that the drift kinetic effects from fast ions lead to very minor change of the mode stability. The reason is the lack of resonances as shown in Fig. 6 in the particle phase space. For fast ions, the wave-particle resonances can occur in the trapping region and near the boundary between the trapping and passing regions. However, in the phase space domain where the resonance is possible, the deposited fast ion density is very low. The fast ions are predominantly deposited in the passing region. Since the mode frequency in the plasma frame, in the $R = 100 - 120$ cm radii, roughly varies between -5 and 5 kHz, we consider three mode frequencies (-5, 0, 5) kHz and find that the resonance between the fast ions and the mode is very weak.

One physics effect that we have neglected is the influence of (fast) plasma flow on the plasma equilibrium, since CHEASE solves for a static equilibrium. On the other hand, the equilibrium reconstruction is made via LRDFIT which includes the MSE constraint for the rotating plasmas in experiments, the possible flow modification to the safety factor is thus taken into account through measurements, albeit not fully consistently. The other important effect of fast flow is to change the plasma density profile, being not a flux function anymore due to centrifugal force. This introduces a finite gradient along the poloidal direction [8], which in theory can induce a second geodesic acoustic mode (GAM) [33]. The presence of this mode generally has a damping effect on the $q = 1$ internal kink mode [34]. On the other hand, so far no experimental observation has been reported in NSTX on the second GAM.

Finally, we point out that there can be several alternative interpretations for this low-f mode observed in NSTX. One possible candidate is the ideal peeling mode [35]. However, the peeling mode interpretation cannot explain the observed mode frequency and mode structure in the plasma core. In experiments, no clear magnetic islands were observed, excluding the

possibility of a tearing mode. The resistive interchange mode is also unlikely, since the D_R index [36] is usually negative ($D_R < 0$) across the whole plasma column for these NSTX plasmas. A global kink mode, such as the resistive wall mode, is easily excluded due to mismatch of the mode frequency as well as the mode structure. Besides, the representative plasma shown in Fig.3 has $\beta_N \approx 2.5$, much below the no-wall beta limit of $\beta_N^{no-wall} \approx 5.2$ computed for this static equilibrium.

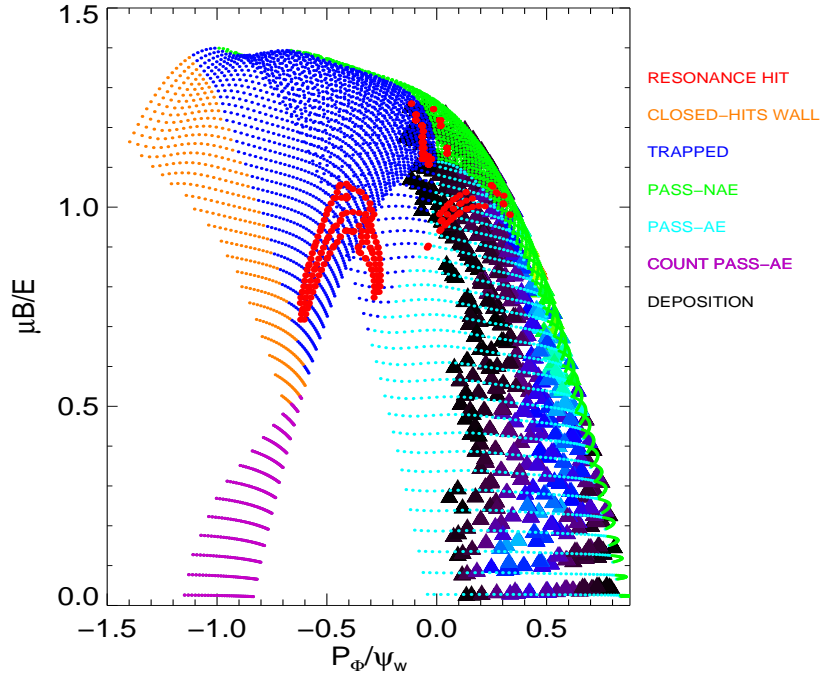


FIG. 6. The resonance condition (red \bullet , labeled by "RESONANCE HIT") between the low-f internal mode and fast ions in the particle phase space. The fast ion energy is fixed at 75 keV. The following aspects are considered: (i) both the toroidal and poloidal frequencies of fast ions are computed; (ii) chosen are three mode frequencies, 0, -5 kHz and 5 kHz, in the plasma frame; (iii) for dumping fast-ion density (\blacktriangle) from TRANSP computations, the spatial region is limited to $0 < s = \sqrt{\psi_p} < \sim 0.5$, being roughly the mode occupation region. Here, the fast ion peak density is normalized to unity, with black color denoting the relative level $< 5\%$. Here, "AE" and "NAE" denotes the orbits that do and do not enclose magnetic axis, respectively. "CLOSED-HITS WALL" denotes the orbits that hit the wall.

Conclusion.—A class of low frequency modes in NSTX are identified as the internal

instability driven by centrifugal force due to fast toroidal flow. Extensive toroidal modeling recovers most features of the mode as observed in experiments, including (i) the mode frequency; (ii) the synthesized diagnostic data measuring the internal mode structure; (iii) the threshold flow speed $\Omega_c \tau_A$ for the mode onset. Furthermore, it is found that the driving mechanism of the mode is robust against uncertainties in constructing the radial profile of the equilibrium safety factor. The mode is located around the location of sharp density gradient. The radial profile of the plasma core density changes the threshold rotation speed $\Omega_c \tau_A$ in certain parameter space. These physics understandings of fast flow driven instabilities are crucial not only for interpreting experimental results, but also for developing advanced research plans in high plasma performance in future experiments such as NSTX-U and MAST-U. More important, since the achievable rotation value on NSTX is comparable with that for future ST-CTF [9], the presented results in this work are helpful for the conceptual design of ST-CTF to avoid the instability driven by fast plasma flow.

We thank Prof. C. Wahlberg for very useful discussions on second GAM and the entire NSTX-U team for their support. This work is supported by the US DOE under Grant Nos. DE-AC02-09CH11466, DE-FG02-06ER54867, and DE-FG03-02ER54681, and also partly supported by the U.S. DoE Office of Science under Contract Nos. DE-FG02-95ER54309 and DE-FC02-04ER54698, and by National Natural Science Foundation of China (No. 11775067).

-
- [1] H.Reimerdes, A.M. Garofalo, G.L. Jackson, M. Okabayashi, *et. al.*, Phys. Rev. Lett. **98**, 055001 (2007).
 - [2] J. Luxon, Nucl. Fusion **42**, 614 (2002).
 - [3] I. Chapman, S. Brown, R. Kemp, and N. Walkden, Nucl. Fusion **52**, 042005 (2012).
 - [4] M. S. Chu, L. Chen, L.-J. Zheng, C. Ren, and A. Bondeson, Nucl. Fusion **39**, 2107 (1999).
 - [5] L.-J. Zheng, M. S. Chu, and L. Chen, Phys. Plasmas **6**, 1217 (1999).
 - [6] P. Helander, R. J. Akers, and L.-G. Eriksson, Phys. Plasmas **12**, 112503 (2005).
 - [7] M. Ono, S.M. Kaye, Y.-K.M. Peng, G. Barnes *et.al.*, Nucl. Fusion **40**, 557 (2000).
 - [8] J.E. Menard, R.E. Bell, E.D. Fredrickson, D.A. Gates *et al.*, Nucl. Fusion **45**, 539 (2005).
 - [9] Y-K M Peng, P J Fogarty, T W Burgess, D J Strickler *et al.*, Plasma Phys. Control. Fusion

- 47**, B263 (2005).
- [10] N. D'Angelo, *The Physics of Fluids* **8**, 1748 (1965).
- [11] A. Miura, *Journal of Geophysical Research: Space Physics* **89**, 801 (1984).
- [12] J. Casanova, J. Jose, E. GarCia-Berro, S. Shore, and A. Calder, *Nature* **478**, 490 (2011).
- [13] B. Levitt, D. Maslovsky, M. E. Mauel, and J. Waksman, *Phys. Plasmas* **12**, 055703 (2005).
- [14] S.S. Medley, N.N. Gorelenkov, R. Andre, R.E. Bell *et al.*, *Nucl. Fusion* **44**, 1158 (2004).
- [15] J.E. Menard R.E. Bell D.A. Gates S.M. Kaye *et al.*, *Phys. Rev. Lett.* **97**, 095002 (2006).
- [16] J.E. Menard S. Gerhardt, M. Bell, J. Bialek *et al.*, *Nucl. Fusion* **52**, 083015 (2012).
- [17] J.E. Menard, Z. Wang, Y. Liu, and R.E. Bell *et al.*, *Phys. Rev. Lett.* **113**, 255002 (2014).
- [18] E.D. Fredrickson, N.N. Gorelenkov, M. Podesta, A. Bortolon *et al.*, *Nucl. Fusion* **54**, 093007 (2014).
- [19] M. Podesta, M. Gorelenkova, D.S. Darrow and E.D. Fredrickson *et al.*, *Nuclear Fusion* **55**, 053018 (2015).
- [20] E. D. Fredrickson, C. Z. Cheng, D. Darrow and G. Fu *et al.*, *Phys. Plasmas* **10**, 2852 (2003).
- [21] R.J Goldston, D.C McCune, H.H Towner, S.L Davis *et.al.*, *J. Comput. Phys.* **43**, 61 (1981).
- [22] M. Podesta, M. Gorelenkova, E. D. Fredrickson, N. N. Gorelenkov *et al*, *Physics of Plasmas* **23**, 056106 (2016).
- [23] R. E. Bell and R. Feder, *Rev. Sci. Instrum.* **81**, 10D724 (2010).
- [24] M. S. Chu, J. M. Greene, T. H. Jensen, R. L. Miller, *et al.*, *Phys. Plasmas* **2**, 2236 (1995).
- [25] Y.Q. Liu, A. Bondeson, M.S. Chu, J.-Y. Favez *et al.*, *Nucl. Fusion* **45**, 1131 (2005).
- [26] H. Lutjens, A. Bondeson, and O. Sauter, *Comput. Phys. Commun.* **97**, 219 (1996).
- [27] J.E. Menard, Homepage for the LRDFIT code, <http://nstx-u.pppl.gov/software/lrdfit>, .
- [28] I. Chapman, M.-D. Hua, S. Pinches, R. Akers, A. Field, J. Graves, R. Hastie, C. Michael, and the MAST Team, *Nucl. Fusion* **50**, 045007 (2010).
- [29] F. Wang, G. Y. Fu, J. A. Breslau, K. Tritz, and J. Y. Liu, *Phys. Plasmas* **20**, 072506 (2013).
- [30] J.A. Breslau, M.S. Chance, J. Chen, G.Y. Fu *et al.*, *Nucl. Fusion* **51**, 063027 (2011).
- [31] L.M. Yu, W. Chen, M. Jiang, Z.B. Shi *et al.*, *Nucl. Fusion* **57**, 036023 (2017).
- [32] Y. Q. Liu, M. S. Chu, I. T. Chapman, and T. C. Hender, *Phys. Plasmas* **15**, 112503 (2008).
- [33] C. Wahlberg, *Phys. Rev. Lett.* **101**, 115003 (2008).
- [34] C. Wahlberg, I. T. Chapman, and J. P. Graves, *Phys. Plasmas* **16**, 112512 (2009).
- [35] A. Bortolon *et al*, 2011, Fast Ion Losses and Redistribution Induced by Low Fre-

quency MHD in NSTX Plasmas, 12th IAEA Technical Meeting on Energetic Particles in Magnetic Confinement Systems, Austin, USA, 8-10 September. <http://www-naweb.iaea.org/napc/physics/meetings/TM40762.html>.

[36] A. Glasser, J. Greene, and J. Johnson, *Phys. Fluids* **18**, 875 (1975).